ARTICLES

Journal of Semiconductors
(2022) 43, 062303
doi: 10.1088/1674-4926/43/6/062303

Optical transmitter module with hybrid integration of DFB laser diode and proton-exchanged $LiNbO_3$ modulator chip

Xuyang Wang[1, 2, 3], He Jia[3], Junhui Li[3], Yumei Guo[3], and Yu Liu[1, †]

[1]State Key Laboratory on Integrated Optoelectronics, Institution of Semiconductors, Chinese Academy of Sciences, Beijing 100083, China

[2]University of Chinese Academy of Sciences, Beijing 100049, China

[3]Beijing Shiweitong Science & Technology Co., Ltd. , Beijing 100176, China

Abstract: In this work, a hybrid integrated optical transmitter module was designed and fabricated. A proton-exchanged Mach–Zehnder lithium niobate ($LiNbO_3$) modulator chip was chosen to enhance the output extinction ratio. A fiber was used to adjust the rotation of the polarization direction caused by the optical isolator. The whole optical path structure, including the laser chip, lens, fiber, and modulator chip, was simulated to achieve high optical output efficiency. After a series of process improvements, a module with an output extinction ratio of 34 dB and a bandwidth of 20.5 GHz (from 2 GHz) was obtained. The optical output efficiency of the whole module reached approximately 21%. The link performance of the module was also measured.

Key words: optical transmitter module; hybrid integration; DFB laser chip; $LiNbO_3$ modulator chip

Citation: X Y Wang, H Jia, J H Li, Y M Guo, and Y Liu, Optical transmitter module with hybrid integration of DFB laser diode and proton-exchanged $LiNbO_3$ modulator chip[J]. *J. Semicond.*, 2022, 43(6), 062303 . https://doi.org/10.1088/1674-4926/43/6/062303

1. Introduction

Lithium niobate ($LiNbO_3$) single crystals have been recognized as the most mature material for electro-optic modulators thanks to their Pockels effect[1]. Compared with modulators based on the carrier effect or microring structures-such as direct modulation lasers[2, 3], InP modulators[4], and silicon-based modulators[5], broadband $LiNbO_3$ Mach–Zehnder (MZ) modulators with the advantages of broad bandwidth, high extinction ratio, very low chirp, and high stability[6] have been widely used in optical communication backbone transmission networks, high-performance broadband optical links, and radio-frequency (RF) photonics, and have attracted considerable attention in the last century. However, the incompatibility between the $LiNbO_3$ chip fabrication process and the complementary metal–oxide–semiconductor (CMOS) process has brought significant obstacles in hybrid integration research based on $LiNbO_3$ modulators. Therefore, few studies have been done in this direction.

In recent years, radio-frequency (RF) photonics technology (e.g., microwave photonics radars and electronic warfare systems) has rapidly matured, and continues to develop toward miniaturization and integration[7]. Most of these systems utilize $LiNbO_3$ modulators to fulfill the requirements for broad bandwidth, high modulation linearity, and good reliability. Therefore, the hybrid integration of a $LiNbO_3$ modulator chip and a laser chip has become a pivotal technology to reduce the volume of the whole system.

The DFB laser chip and the $LiNbO_3$ modulator chip are made of different materials. Several methods can be used to integrate laser chips and modulator chips, such as via lenses[8], through edge coupling[9, 10], through vertical coupling[11, 12], bonding InP chips to Si substrates[13], utilizing heteroepitaxial growth[14], using planar lightwave circuits (PLCs)[15], and so on. Considering the performance, fabrication feasibility, and production cost, in this work a hybrid integrated optical transmitter module was realized by coupling the laser and $LiNbO_3$ modulator via a lens.

2. Schematic design

The layout of the transmitter module is illustrated in Fig. 1. The module comprises a laser chip unit, a lens, an optical isolator, a broadband $LiNbO_3$ Mach–Zehnder modulator chip unit, and fibers. The housing material is Kovar. The size of the whole package is minimized by design.

The laser unit includes a distributed feedback (DFB) laser chip, a monitor photodetector (PD), a thermistor, and a control circuit. The laser chip unit is installed with a heat sink and TEC (Thermo Electric Cooler). The DFB laser works with stable wavelength and stable power under the control of the current and the TEC through the real-time feedback of the monitor PD and the thermistor[16]. Fig. 2 shows the structure of the DFB laser chip unit.

The light emitted by the DFB laser chip is coupled to the input optical waveguide of the modulator chip through a spatial lens, an optical isolator, and a fiber-tail. The modulator chip unit comprises a microstrip, a $LiNbO_3$ modulator chip, a photodetector, and a bias control circuit, as shown in Fig. 3.

The radio frequency (RF) signal is loaded to the modulator chip through a microwave connector and a microstrip on the shell, connecting the RF connector and the modulator chip electrode. A traveling-wave electrode structure is adopted on the modulator chip[17] to increase the modulation bandwidth.

Correspondence to: Y Liu, yliu@semi.ac.cn
Received 6 DECEMBER 2021; Revised 25 FEBRUARY 2022.

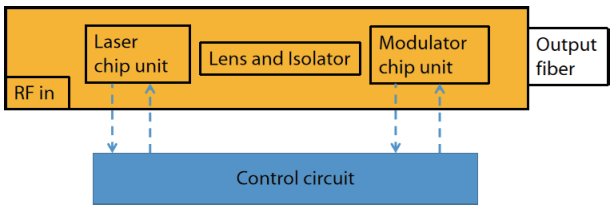

Fig. 1. (Color online) Diagrammatic sketch of the module.

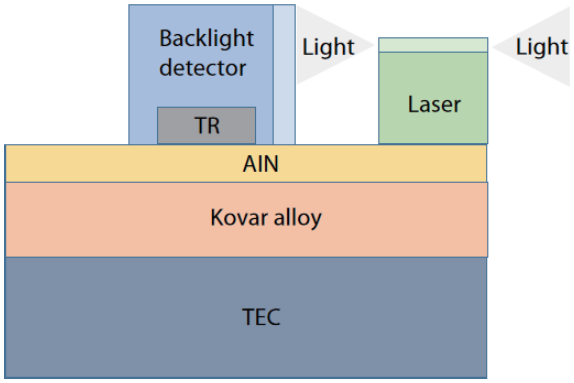

Fig. 2. (Color online) Diagrammatic sketch of the laser chip unit.

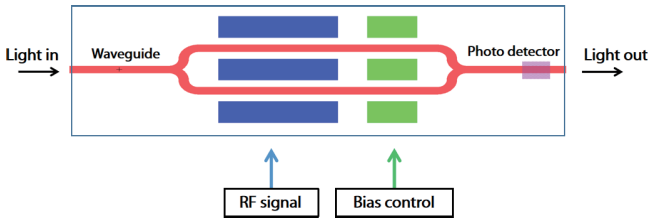

Fig. 3. (Color online) Sketch of the modulator chip unit.

The $LiNbO_3$ Mach–Zehnder modulator must work at the quadrature point[18] to achieve the maximum gain of the transmitter. Therefore, a bias control circuit based on the pilot method[19] or the power-monitor method[20] is required to adjust the bias voltage of the modulator in real-time. A bottom light-incoming photodetector is placed on the waveguide of the modulator chip to monitor the output optical signal in real-time and send it to the bias control circuit. The modulator bias control circuit and the DFB laser control circuit are integrated on a PCB board to minimize the size of the module.

The output light beam of the modulator chip is coupled into an optical fiber that is attached to the output end of the modulator chip and it then goes out from the whole module.

3. Simulation

The simulation consists of two parts: the optical path design and the modulator chip design. The positions and parameters of each optical unit (e.g., the lens, isolator, and fiber) were optimized to maximize the optical output efficiency of the whole module. The modulator chip's waveguide and traveling-wave electrode structure were also designed to obtain a high on-off extinction ratio, a wide bandwidth, and a low insertion loss.

Fig. 4 shows the optical coupling path of the module. The output beam from the laser chip goes through a subassembly comprising a microlens and a microisolator, which rotates the polarization direction of the light by 45°.

There are several mature $LiNbO_3$ waveguide fabrication

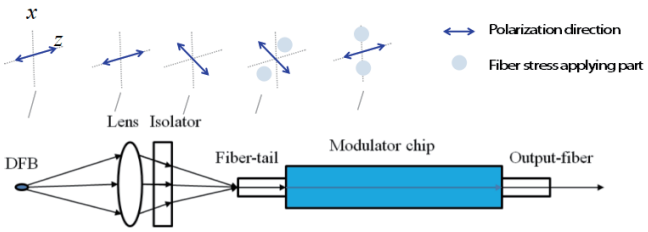

Fig. 4. (Color online) Optical path of the module.

methods, such as the ridge waveguide method[21], titanium diffusion method[22], and proton exchange method[23]. The ridge waveguide and titanium diffusion waveguide transmit dual-polarized directional light, while the proton exchange waveguide substantially filters out all but a single linear polarization of light. Since γ_{33} is the largest electro-optic coefficient of the $LiNbO_3$ single crystal[24], it is desirable to apply both the electric field direction and the incident optical wave polarization direction along the z-axis of the $LiNbO_3$ crystal to increase the modulation efficiency. The light polarized in the nonworking direction cannot be transmitted due to the polarization selectivity of the proton-exchange waveguide, which improves the output extinction ratio of the module and eliminates the errors caused by interactions among waves of different polarizations. However, the rotation of the light polarization direction caused by the isolator will lead to an extra optical coupling loss. A small section of twisted polarization maintaining fiber (Corning PM15-U25D) was added to solve this problem in our work. As shown schematically in Fig. 4, the light polarization direction is rotated by 45° after the isolator and then rotated back by the twisted fiber. The coupling efficiency reaches maximum when the polarization direction of the light in the fiber is along the TE mode of the modulator chip. Fig. 5(a) shows the dependence of the final optical output efficiency on the angle shift of the light polarization direction caused by the rotation of the fiber. The maximum optical output efficiency occurs when the fiber is rotated by 45°. The length of the fiber is about 15 mm for packaging needs.

The parameters and positions of the laser chip, the lens, and the fiber (e.g., the numerical aperture and focal length of the lens) are calculated and optimized to achieve the maximum optical output efficiency. The optical axis of each component must be strictly located in a straight line to avoid the optical loss caused by the offset of each unit. Figs. 5(b) and 5(c) shows the optical output efficiency's dependence on the optical axis offset of the lens and the fiber to the cocenter optical axis of the whole module.

What can be observed and inferred from Figs. 5(b) and 5(c) is that the optical output efficiency is much more sensitive to the optical axis offset of the lens than the fiber. Therefore, the micro-assembly technology of the lens would be the critical point of module fabrication.

The optical output efficiency is also influenced by the mode field diameter (MFD) of the modulator waveguide, as shown in Fig. 5(d). The MFD of the communication fiber is approximately 10 μm, and the optical output efficiency reaches the maximum point when the MFD of the modulator waveguide is the same as that of the fiber. The mismatch of the MFD between the modulator waveguide and the fiber introduces extra coupling loss between the modulator chip and the fiber.

To obtain a high output extinction ratio of the module,

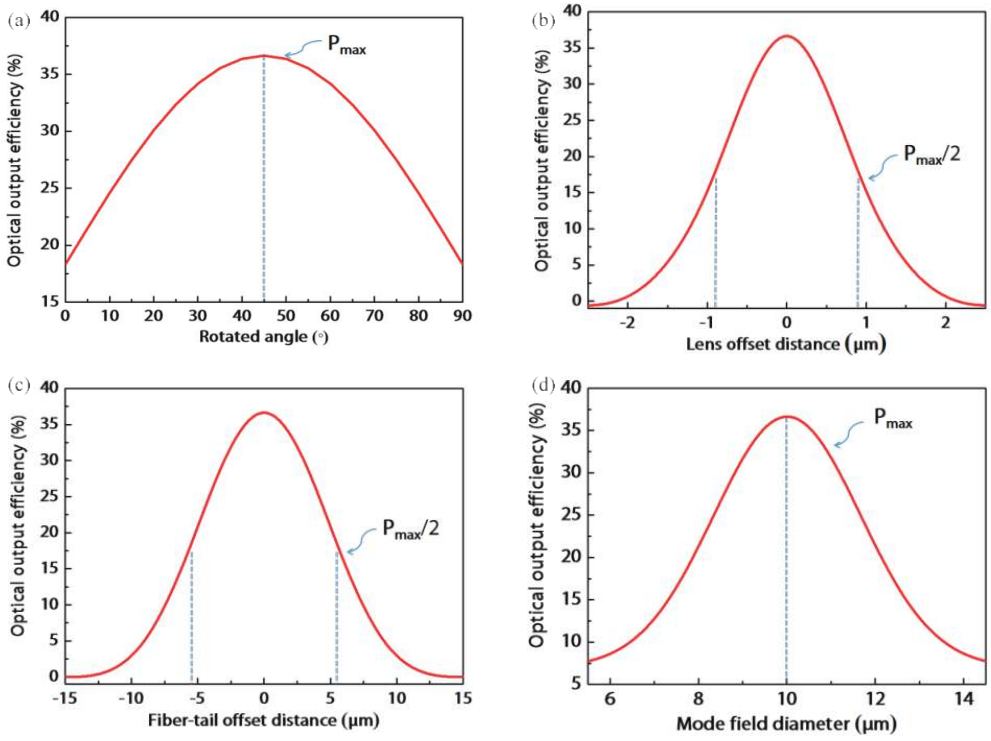

Fig. 5. (Color online) Simulation results of normalized optical output efficiency of the module vs. (a) rotated angle of the fiber, (b) optical axis offset distance of the lens, (c) optical axis offset distance of the fiber to the cocenter optical axis, and (d) the MFD of the modulator waveguide.

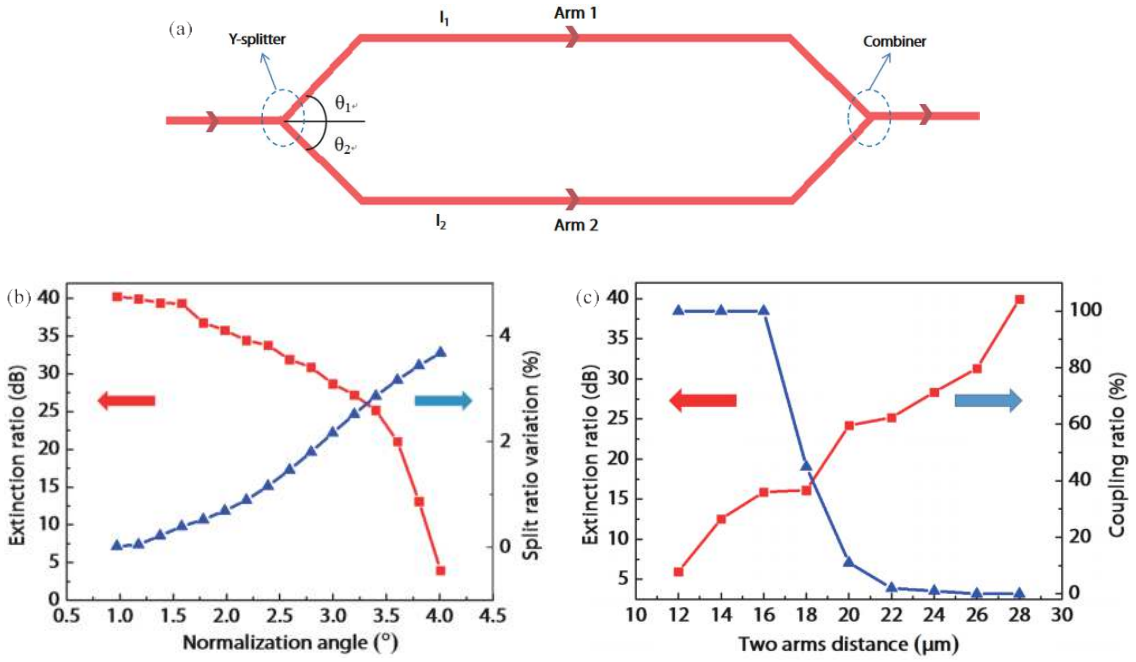

Fig. 6. (Color online) (a) MZ-modulator waveguide structure. (b) Simulation results of extinction ratio (on/off) and split ratio variation vs. normalization angle. (c) Simulation results of extinction ratio (on/off) and coupling ratio vs. two arms distance.

the waveguide structure of the modulator should be well designed. The extinction ratio of the $LiNbO_3$ modulator mainly depends on the optical intensity balance and coupling ratio between the two modulation arms. Fig. 6(a) is a schematic drawing of the MZ waveguide structure of the modulator. The incoming light signal splits into two arms through a Y-splitter. The optical intensity in Arm 1 is I_1, and that in Arm 2 is I_2. The angles between the input light signal and each Y-branch are θ_1 and θ_2, respectively. The optical phase in each arm can be modulated by an applied voltage. The in-phase traveling through the two arms will result in a maximum intensity output, while the out-phase traveling will result in a minimum intensity output after the combiner[1].

Fig. 6(b) shows the relationship between the extinction ratio and the split ratio variation. The split ratio variation is defined as $|(I_1 - I_2)/(I_1 + I_2)|$, and the normalization angle is defined as $|\theta_1 - \theta_2|$. When θ_1 equals θ_2, the input optical intensity splits evenly into Arm 1 and Arm 2. The modulator's

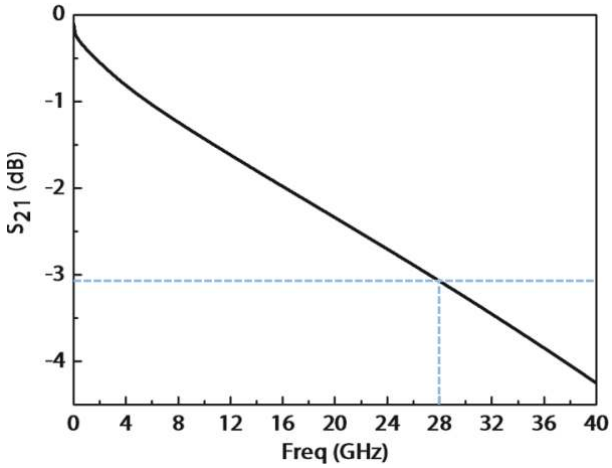

Fig. 7. Simulation results of the electro-optic response of the module.

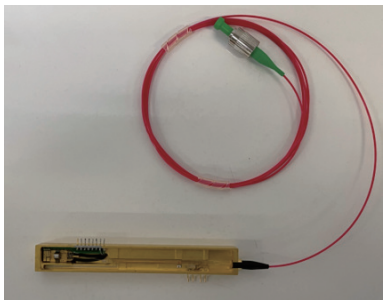

Fig. 8. (Color online) Hybrid integrated optical transmitter module.

on/off extinction ratio reaches maximum. Fig. 6(c) shows the relationship between the extinction ratio and the optical power coupling ratio of the two modulator arms. When the optical powers of the two modulation arms couple, the extinction ratio decreases.

The module's bandwidth depends on the bandwidth of the modulator chip and the RF transmission loss of the microstrip line. The design of the traveling-wave electrode and the microstrip line should be optimized to satisfy the required bandwidth. Fig. 7 shows the simulated result of the electro-optic response of the module. The bandwidth of the module could reach up to 28 GHz.

4. Results and discussion

According to the assembly requirements of each unit, the sequence to construct the module was optimized as follows. First, the laser chip, monitor PD, and thermistor were mounted on the same heat sink and TEC. Then, the laser module was assembled into the designed shell. The laser chip control circuit was also connected. The modulator chip was coupled with the input and output fiber. It was then installed in the shell, connected with the modulator bias-control circuit. The hybrid integrated optical transmitter module is shown in Fig. 8. Online monitoring of the output optical power of the whole module was allowed. The maximum output optical power of the module was realized by constantly adjusting the position of the lens and isolator.

The DFB laser chip was able to provide over 70 mW of optical power with fewer than 1 MHz linewidths. Fig. 9 shows the tested characteristic curve of the laser chip.

The waveguide of the modulator chip was fabricated using the proton exchange and annealing method. By adjusting the temperature and time of the process, the MFD of the waveguide approached the designed value. The overall insertion loss of the chip was 3.6 dB with both the input and output ends coupled with the polarization-maintaining single-mode fibers (PMSMF).

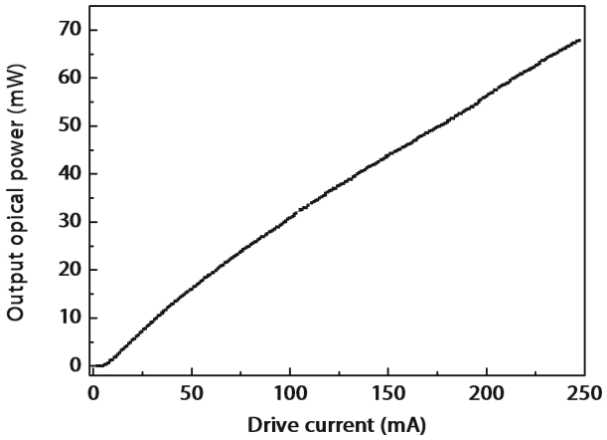

Fig. 9. *P*–*I* curve of the DFB laser chip.

By continuously optimizing the chip structure and the fabrication process (e.g., the Y-branch structures of the waveguide, the photolithography process, and the electroplating process), the electro-optic (EO) bandwidth of the modulator chip reached 26.5 GHz (from 2 GHz) at 3 dB and the extinction ratio (ER) of the chip was better than 35 dB. The test results are shown in Fig. 10.

The optical output efficiency of the module obtained by simulation was 42.3%. However, the measured optical output efficiency was approximately 21%, as shown in Table 1. The reason for this may be that the parameters used in the simulation, such as the divergence angle of the laser and numerical aperture of the lens, were slightly different from the actual parameters. The inevitable offset of each unit and inaccurate tilted angle of the fiber during fabrication would also lead to a large deviation in the overall results.

The output optical power of the module depends on the optical power provided by the laser chip, the coupling loss from the laser chip to the fiber-tail, and the insertion loss of the modulator chip. In this work, the laser chip with 600 μm cavity length provides power over 70 mW, the coupling loss is about 3.2 dB, while the insertion loss is 3.6 dB. In future work, the following methods could be helpful to increase the output power of the module: applying higher power laser chips with longer cavity length, increasing the coupling efficiency by selecting the lens parameters in accordance with the actual divergence angle of the laser chip, or decreasing the insertion loss by optimizing the modulator chip's waveguide fabrication process to make the waveguide's mode field diameter match better with that of the optical fiber.

The measured bandwidth was 20.5 GHz (from 2 GHz), which is 6 GHz smaller than the modulator chip bandwidth caused by the microwave transmission loss along the microstrip. Fig. 11(a) shows the tested result. The difference between the simulation and the tested result was mainly caused by the deviations and defects of the modulator electrode structures and microstrip line during fabrication. The extinction ratio of the module was 34 dB, which is slightly smaller than that of the modulator chip. This might be due to the

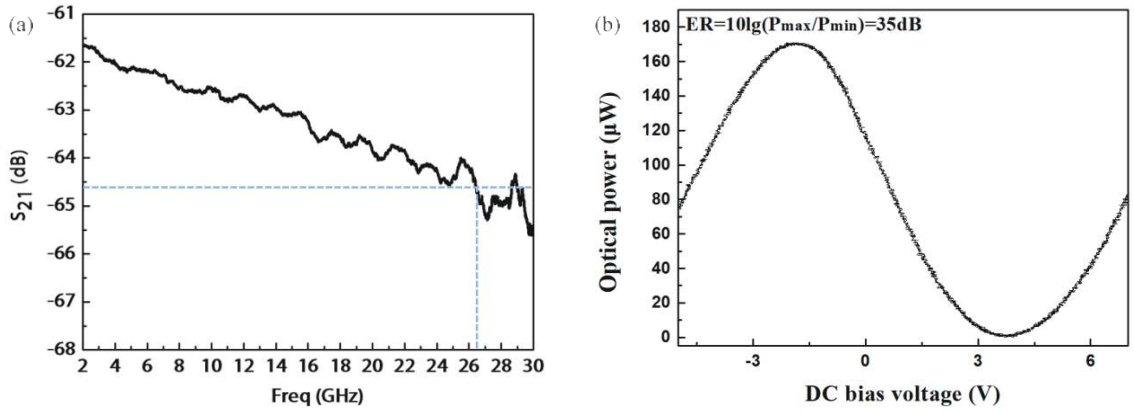

Fig. 10. (a) EO bandwidth and (b) ER test results of the $LiNbO_3$ modulator chip.

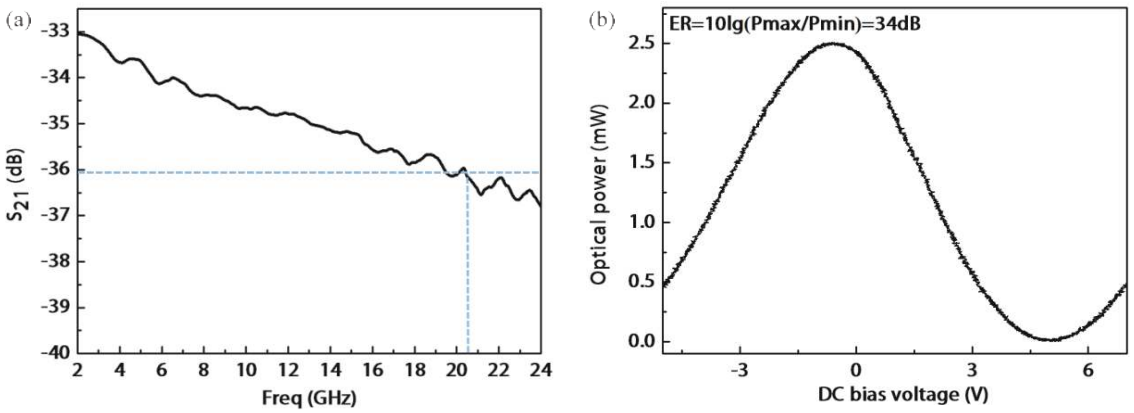

Fig. 11. (a) EO bandwidth and (b) ER test results of the module.

Table 1. Test results of the optical output efficiency.

Laser's drive current (mA)	Laser's power (mW)	Module's power (mW)	Optical output efficiency (%)
50.80	16.60	3.45	20.78
101.00	31.10	6.60	21.22
200.00	56.30	12.15	21.58
227.00	63.10	13.70	21.71

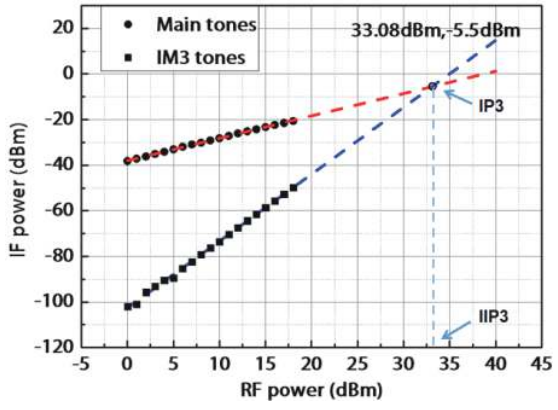

Fig. 12. (Color online) Output RF power of a linear tone and of a third-order intermodulation vs. the RF input power.

different measurement setups.

The transmitter module's link p erformance parameters were also tested by connecting the transmitter module to a microwave system. When the input RF signal was 9 GHz, the noise figure (NF) of the system was 38.81 dB. The 1 dB compression point ($P_{1\ dB}$) was 19.5 dBm. The 3rd-order intercept point (IIP_3) was 33.08 dBm, as shown in Fig. 12. The 3rd-order spur free dynamic range ($SFDR_3$), which characterizes the linearity behavior of the module, can be shown to be equal to

$$\mathrm{SFDR_3} = \frac{2}{3}[\mathrm{IIP_3} - \mathrm{NF} - (-174)]\,\mathrm{dB}\cdot\mathrm{Hz}^{\frac{2}{3}}] = 112\,\mathrm{dB}\cdot\mathrm{Hz}^{\frac{2}{3}}. \quad (1)$$

These performance metrics are consistent with those of a discrete system with identical test conditions.

$SFDR_3$ is an essential parameter for analog modulation links. It can be improved by using a higher power and lower relative intensity noise laser chip, increasing the V_π of the modulator chip appropriately, raising the optical coupling efficiency, and so on. However, increasing the modulator's V_π will reduce the link's gain. Therefore, comprehensive consideration including the gain, noise figure, and $SFDR_3$ should be taken according to the requirements of the system's applications.

5. Conclusion

By packaging the DFB laser chip and the $LiNbO_3$ Mach–Zehnder modulator chip in one shell, a hybrid integrated optical transmitter module was realized with a significant reduction in volume compared to existing systems based on discretely packaged components. Moreover, by adopting the proton-exchange $LiNbO_3$ waveguide fabrication scheme and optimizing the $LiNbO_3$ waveguide structure and fabrica-

tion process, the extinction ratio of the module reaches 34 dB, while the typical extinction ratio of a discrete system is approximately 20 dB. The optical output efficiency of the hybrid integrated optical transmitter module reached approximately 21% with a 3 dB bandwidth of 20.5 GHz (from 2 GHz). The link performance parameters of the hybrid integrate module are comparable to those of a discrete system with identical test conditions. In the next stage, we will focus on the environmental adaptability of the transmitter module and its characteristics in the system.

Acknowledgements

This work was supported by National Key Research and Development Program of China (2018YFB2201101), the Strategic Priority Research Program of Chinese Academy of Sciences，Grant No. XDB43000000 and Beijing Municipal Science & Technology Commission，Administrative Commission of Zhongguancun Science Park No. Z201100004020004

References

[1] Li G L, Yu P K L. Optical intensity modulators for digital and analog applications. J Lightwave Technol, 2003, 21, 2010

[2] Dagli N. Wide-bandwidth lasers and modulators for RF photonics. IEEE Trans Microw Theory Tech, 1999, 47, 1151

[3] Huang J N, Li C, Lu R G, et al. Beyond the 100 Gbaud directly modulated laser for short reach applications. J Semicond, 2021, 42, 041306

[4] Liu D P, Tang J, Meng Y, et al. Ultra-low V_{pp} and high-modulation-depth InP-based electro–optic microring modulator. J Semicond, 2021, 42, 082301

[5] Wang X X, Weigel P O, Zhao J, et al. Achieving beyond-100-GHz large-signal modulation bandwidth in hybrid silicon photonics Mach Zehnder modulators using thin film lithium niobate. APL Photonics, 2019, 4, 096101

[6] Wooten E L, Kissa K M, Yi-Yan A, et al. A review of lithium niobate modulators for fiber-optic communications systems. IEEE J Sel Top Quantum Electron, 2000, 6, 69

[7] Marpaung D, Roeloffzen C, Heideman R, et al. Integrated microwave photonics. Laser Photonics Rev, 2013, 7, 506

[8] Lu Z Y, B Lu, Luo Y, et al. Design and research on small hybrid integrated teansmitter module of semiconductor and DFB laser. J Opto Laser, 2021, 32, 181

[9] Li Y, Lan T, Li J, et al. High-efficiency edge-coupling based on lithium niobate on an insulator wire waveguide. Appl Opt, 2020, 59, 6694

[10] Li L Y, Ma Y X, Zhang Y S, et al. Multi-tip edge coupler for integration of a distributed feedback semiconductor laser with a thin-film lithium niobate modulator. Appl Opt, 2021, 60, 4814

[11] Qiu M. Vertically coupled photonic crystal optical filters. Opt Lett, 2005, 30, 1476

[12] Chakravarty S, Teng M, Safian R, et al. Hybrid material integration in silicon photonic integrated circuits. J Semicond, 2021, 42, 041303

[13] Matsumoto K, Kanaya Y, Kishikawa J, et al. Characteristics of film InP layer and Si substrate bonded interface bonded by wafer direct bonding. 2015 11th Conference on Lasers and Electro-Optics Pacific Rim, 2015, 7375926

[14] Olmstead M A, Ohuchi F S. Group III selenides: Controlling dimensionality, structure, and properties through defects and heteroepitaxial growth. J Vac Sci Technol A, 2021, 39, 020801

[15] Okamoto K. Fundamentals of optical waveguides. 2nd ed. Elsevier Inc. , 2006

[16] Zhang J, Gao C X, Xue M Y, et al. Research on frequency modulation character of the current driven DFB semiconductor laser. Mod Phys Lett B, 2019, 33, 1850422

[17] Alferness R C. Waveguide electrooptic modulators. IEEE Trans Microwave Theory Tech, 1982, 30, 1121

[18] Tan J, Chen X, Liu X, et al. Research on a bias control technique for quadrature-point locking in $LiNbO_3$ MZ modulators. Semicond Optoe, 2018, 39(4), 575

[19] Walton J R, Smee E J, Malladi D P. Pilot transmission schemes for wireless multi-carrier communication systems. USA Patent, US7280467, 2007

[20] Wang L L, Kowalcyzk T. A versatile bias control technique for any-point locking in lithium niobate Mach –Zehnder modulators. J Lightwave Technol, 2010, 28, 1703

[21] Yang G, Sergienko A V, Ndao A. Tunable polarization mode conversion using thin-film lithium niobate ridge waveguide. Opt Express, 2021, 29, 18565

[22] Fukuma M, Noda J. Optical properties of titanium-diffused $LiNbO_3$ strip waveguides and their coupling-to-a-fiber characteristics. Appl Opt, 1980, 19, 591

[23] Paz-Pujalt G R, Tuschel D D, Braunstein G, et al. Characterization of proton exchange lithium niobate waveguides. J Appl Phys, 1994, 76, 3981

[24] Méndez A, de la Paliza G, García-Cabañes A, et al. Comparison of the electro-optic coefficient r_{33} in well-defined phases of proton exchanged $LiNbO_3$ waveguides. Appl Phys B, 2001, 73, 485

Xuyang Wang was born in Shandong, China, in 1983. She is a Doctor student at the Institution of Semiconductors and an R&D Manager in Beijing Shiweitong Science Technology Co., Ltd, Beijing, China. She has over ten years of experience in research and development in $LiNbO_3$ modulators. Her research now focuses bandwidth $LiNbO_3$ modulators and hybrid integrated modules.

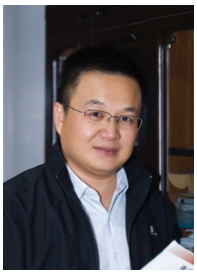

Yu Liu was born in Hunan. China, in 1976. He received the M.S. and Ph.D. degrees in microelectronics and solid-state electronics from the Institute of Semiconductors, Chinese Academy of Sciences (CAS), Beijing, in 2004 and 2008, respectively. He is currently a Full Professor with the Institute of Semiconductors, CAS. His research interests include high-frequency characteristics of microwave optoelectronic devices and design of high-speed optical transceiver modules.